# Effective Three-Body Nuclear Systems with Short-Range Interactions

Jared Vanasse

Ohio University

October 25, 2016

# Effective (Field) Theories

- Disparate scales can be used as an expansion parameter $\lambda_1 \gg \lambda_2, Q \sim \frac{\lambda_2}{\lambda_1}$
- Only valid in regimes where $Q < 1$.

  **Example 1:** For objects a height $h$ above earth the gravitational potential is given by

  $$\Phi(r) = -\frac{GM_E m}{R_E}\left(1 - \frac{h}{R_E} + \left(\frac{h}{R_E}\right)^2 + \cdots\right)$$

  where $Q = \frac{h}{R_E}$ is a small parameter.

  **Example 2:** For thin sheets one can use $Q = t\kappa$ where $t$ is the thickness and $\kappa$ the curvature.

- Effective (field) theories have "power counting" that organizes relative importance of terms. Gives error estimate of calculations.

# Universality at Low Energies

- If $r$ is the typical range of a short range potential. Then for small energies $(E \leq 1/r)$ we can approximate using contact potentials.
- This is a useful description in cold atoms, halo nuclei, low energy nuclear interactions, and etc.

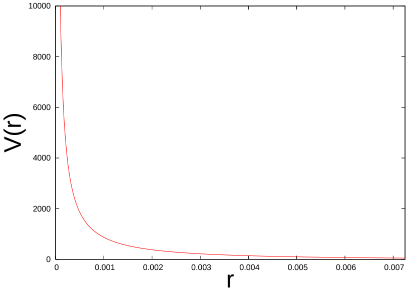


$$\mathcal{F}\left[\frac{1}{|\mathbf{r}|}e^{-m_\pi|\mathbf{r}|}\right] = \frac{1}{\mathbf{q}^2 + m_\pi^2}$$

$$\frac{1}{\mathbf{q}^2 + m_\pi^2} = \frac{1}{m_\pi^2} - \frac{\mathbf{q}^2}{m_\pi^4} + \frac{\mathbf{q}^4}{m_\pi^6} + \cdots$$

$$\mathcal{F}\left[\frac{1}{m_\pi^2} - \frac{\mathbf{q}^2}{m_\pi^4} + \frac{\mathbf{q}^4}{m_\pi^6} + \cdots\right] = \frac{1}{m_\pi^2}\delta^3(\mathbf{r}) - \frac{1}{m_\pi^4}\nabla^2\delta^3(\mathbf{r}) + \frac{1}{m_\pi^6}\nabla^4\delta^3(\mathbf{r}) + \cdots$$

# Recipe for EFT($\not\pi$)

- For momenta $p < m_\pi$ pions can be integrated out as degrees of freedom and only nucleons and external currents are left.
- Write down all possible terms of nucleons and external currents that respect symmetries (rotational, isospin).
- Develop a power counting to organize terms by their relative importance.
- Calculate respective observables up to a given order in the power counting.

# Two-Body Inputs of EFT($\not\pi$)

Expansion parameter in EFT($\not\pi$) $\lambda = \frac{Q}{\Lambda_{\not\pi}}$, where $Q \sim p \sim \frac{1}{a_1}$ and $\Lambda_{\not\pi} \sim m_\pi$
Two-body inputs for EFT($\not\pi$):

- LO scattering lengths in $a_1$ ($^3S_1$) and $a_0$ ($^1S_0$) **non-perturbative**
- NLO range corrections $r_1$ and $r_0$ **perturbative**
- $\mathrm{N^2LO}$ SD-mixing term **perturbative**
- $\mathrm{N^2LO}$ isospin splitting $\Delta_s$ in *nn* and *np* $a_0$ **perturbative**
- $\mathrm{N^3LO}$ shape parameter corrections $s_1$ and $s_0$ **perturbative**
- $\mathrm{N^3LO}$ two-body P-wave contributions $(^3P_J, {}^1P_1)$ **perturbative**

Total of **4** NNLO two-body parameters, ignoring SD and $\Delta_s$.
Total of **12** $\mathrm{N^3LO}$ two-body parameters.

The LO dressed deuteron propagator is given by a bubble sum

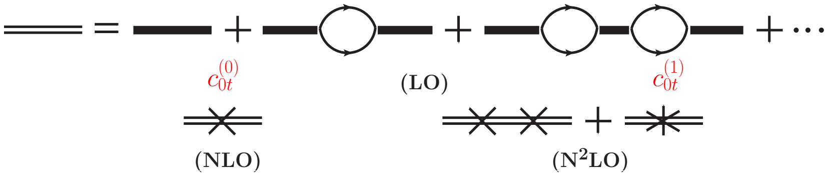


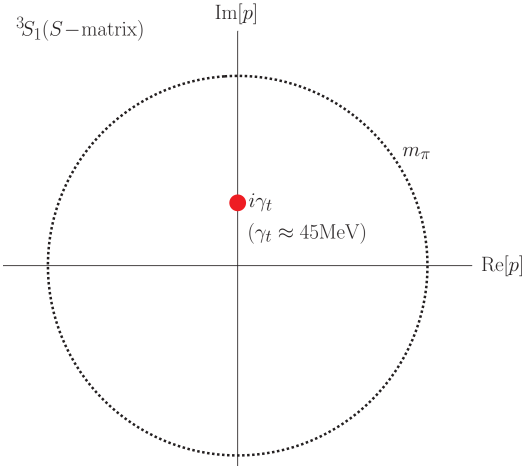


($Z$-parametrization) At LO coefficients are fit to reproduce the deuteron pole and at NLO to reproduce the residue about the deuteron pole (Phillips et al. (2000)).

# Doublet S-wave and Bound state

The three-body Lagrangian is

$$\mathcal{L}_3 = \hat{\psi}^\dagger \left[ \Omega - h_2(\Lambda) \left( i\partial_0 + \frac{\vec{\nabla}^2}{6M_N} + \frac{\gamma_t^2}{M_N} \right) \right] \hat{\psi} + \sum_{n=0}^{\infty} \left[ \omega_{t0}^{(n)} \hat{\psi}^\dagger \sigma_i \hat{N} \hat{t}_i - \omega_{s0}^{(n)} \hat{\psi}^\dagger \tau_a \hat{N} \hat{s}_a \right] + \mathrm{H.c.}.$$

where $\psi$ is an auxiliary triton field. The LO triton vertex function $\mathcal{G}_0(E, p)$ is given by following coupled integral equations (Hagen, Hammer, and Platter (2013))

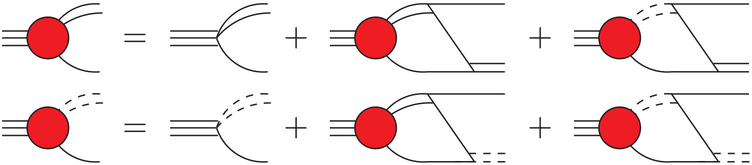

Inhomogeneous term is set to **1** to factor three-body forces out of vertex functions.

# Higher-Order Triton Vertex Function

The NLO ($\mathcal{G}_1(E,p)$) and NNLO ($\mathcal{G}_2(E,p)$) triton vertex functions are

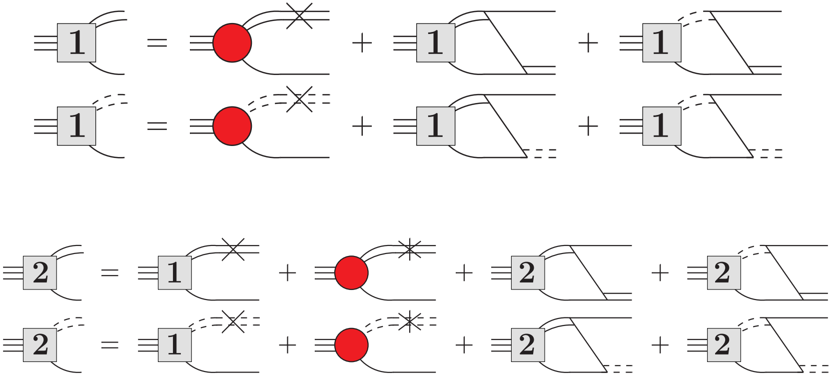

# LO Triton Propagator

Defining

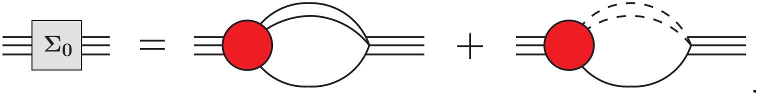


The dressed triton propagator is given by the sum of diagrams


which yields

$$i\Delta_3(E) = \frac{i}{\Omega} - \frac{i}{\Omega}H_{\mathrm{LO}}\Sigma_0(E)\frac{i}{\Omega} + \cdots$$
$$= \frac{i}{\Omega}\frac{1}{1 - H_{\mathrm{LO}}\Sigma_0(E)},$$

where

$$H_{\mathrm{LO}} = -\frac{8\omega_t^2}{\pi\Omega} = -\frac{8\omega_s^2}{\pi\Omega} = \frac{8\omega_t\omega_s}{\pi\Omega}.$$

# Higher-Order Triton Propagator

Defining the functions

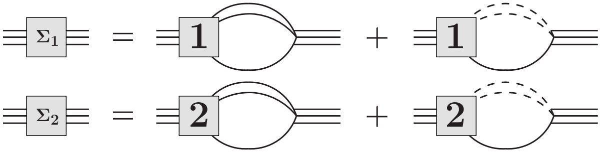


The NNLO triton propagator is


(NLO)

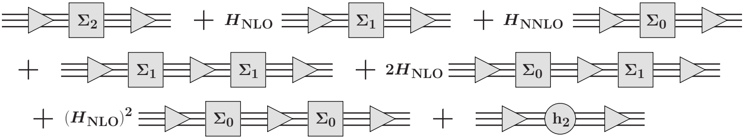


(NNLO)

# Properly Renormalized Vertex Function

- Three-body forces are fit to ensure triton propagator has pole at triton binding energy.
- Triton wavefunction renormalization given by the residue of the triton propagator about the pole.
- LO triton wavefunction renormlization is

$$Z_\psi^{\mathrm{LO}} = \frac{\pi}{\Sigma_0'(B)}.$$

- NNLO three-body, $h_2$ force fit to doublet $S$-wave $nd$ scattering length
- Total of **2** three-body inputs at NNLO.

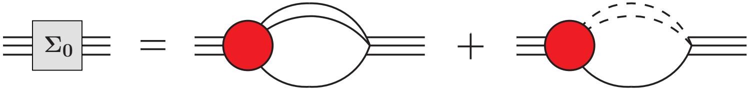

# Triton Charge Form Factor

Charge form factor of triton at LO given by three diagrams

$$\hat{N}^\dagger \left[ i\partial_0 + ie \left( \frac{1+\tau_3}{2} \right) \hat{A}_0 \right] \hat{N}$$

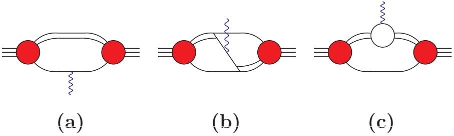


NLO and NNLO triton charge form factor

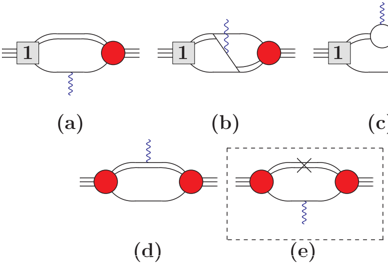


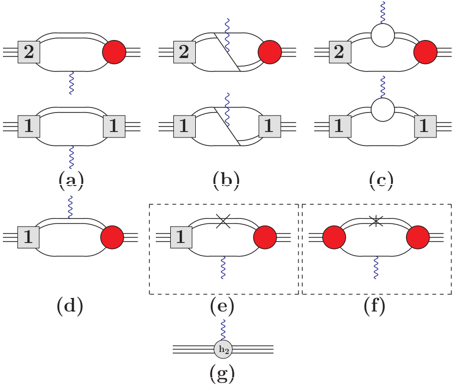

# Form Factors

Charge form factor gives

$$F_C(Q^2) = Z\left(1 - \frac{\langle r_C^2\rangle}{6}Q^2 + \cdots\right)$$

LO EFT($\not{\pi}$) magnetic form factor is given by replacing Coulomb photons with magnetically coupled photons

$$\mathcal{L}_m = \hat{N}^\dagger(\kappa_0 + \tau_3\kappa_1)\boldsymbol{\sigma}\cdot\mathbf{B}\hat{N}$$

Magnetic form factor gives

$$F_m(Q^2) = \mu\left(1 - \frac{\langle r_m^2\rangle}{6}Q^2 + \cdots\right)$$

# Triton Charge Radius

LO EFT($\not\pi$) $r_C = 2.1 \pm .6$ fm (Platter and Hammer (2005))
NLO EFT($\not\pi$) $r_C = 1.6 \pm .2$ fm (Kirscher et *al.* (2005))
NNLO EFT($\not\pi$) $r_C = 1.62 \pm .03$ fm (Vanasse (2016))

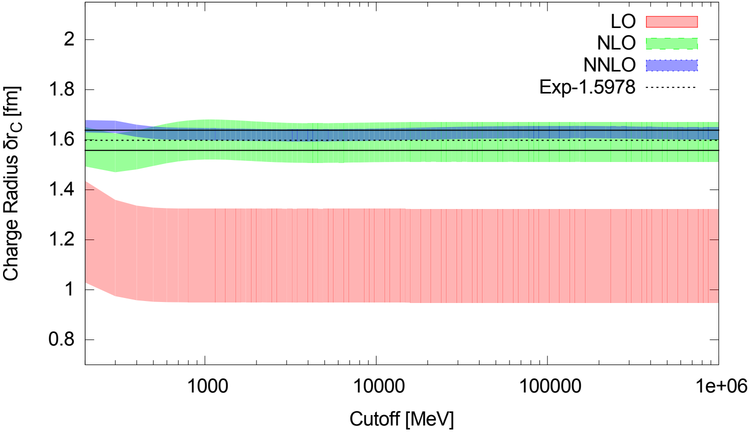

# Bound State Observables for 3$N$ Systems

Partly work in progress (Vanasse (2016)).

| Observable | LO | NLO | NNLO | Exp. |
|---|---|---|---|---|
| $^3$H: $r_C$ [fm] | 1.14(19) | 1.59(8) | 1.62(3) | 1.5978(40) |
| $^3$He: $r_C$ [fm] | 1.26(21) | 1.72(8) | 1.74(3) | 1.7753(54) |
| $^3$H: $r_m$ [fm] | 1.49(22) | WIP | – | 1.840(181) |
| $^3$He: $r_m$ [fm] | 1.58(24) | WIP | – | 1.965(153) |
| $^3$H: $\mu_m$ [$\mu_N$] | 2.75(92) | WIP | – | 2.98 |
| $^3$He: $\mu_m$ [$\mu_N$] | -1.87(62) | WIP | – | -2.13 |

# Consequences of Wigner-symmetry and Unitarity

**Wigner-limit:** $a_0 = a_1$ and $r_0 = r_1$
**Unitary limit:** $a_0 = a_1 = \infty$
**Wigner-breaking $\mathcal{O}(\delta)$:** $\delta = \frac{1/a_1 - 1/a_0}{1/a_1 + 1/a_0}$
**Wigner-breaking all orders:**

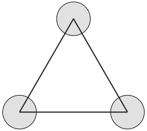

| | Unitary | Wigner | $\mathcal{O}(\delta)$ | $\delta$ all orders |
|---|---|---|---|---|
| LO EFT($\not\pi$) | 1.10 | 1.22 | 1.08/1.19 | 1.14/1.26 |
| $\mathcal{O}(r)$ | 1.42 | 1.66 | 1.58/1.70 | 1.59/1.72 |
| Experiment | | | | 1.5978(40)/1.775(5) |

Table: $^3$H/$^3$He charge radius in unitary and Wigner-limit (Vanasse and Phillips (2016)) arXiv:1607.08585

In Wigner-limit it can be shown both analytically and numerically

$$\mu_{(^3\mathrm{H})} = \mu_p = 2.79\frac{e}{2M_N} \quad , \quad \mu_{(^3\mathrm{He})} = \mu_n = -1.91\frac{e}{2M_N}$$

# Consequences of Wigner-symmetry and Unitarity

**Wigner-limit:** $a_0 = a_1$ and $r_0 = r_1$
**Unitary limit:** $a_0 = a_1 = \infty$
**Wigner-breaking $\mathcal{O}(\delta)$:** $\delta = \frac{1/a_1 - 1/a_0}{1/a_1 + 1/a_0}$
**Wigner-breaking all orders:**

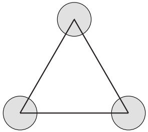

| | Unitary | Wigner | $\mathcal{O}(\delta)$ | $\delta$ all orders |
|---|---|---|---|---|
| LO EFT($\not\pi$) | 1.10 | 1.22 | 1.08/1.19 | 1.14/1.26 |
| $\mathcal{O}(r)$ | 1.42 | 1.66 | 1.58/1.70 | 1.59/1.72 |
| Experiment | | | | 1.5978(40)/1.775(5) |

Table: $^3$H/$^3$He charge radius in unitary and Wigner-limit (Vanasse and Phillips (2016)) arXiv:1607.08585

In Wigner-limit it can be shown both analytically and numerically

$$\mu_{(^3\mathrm{H})} = \mu_p = 2.79\frac{e}{2M_N} \quad , \quad \mu_{(^3\mathrm{He})} = \mu_n = -1.91\frac{e}{2M_N}$$

# Consequences of Wigner-symmetry and Unitarity

**Wigner-limit:** $a_0 = a_1$ and $r_0 = r_1$
**Unitary limit:** $a_0 = a_1 = \infty$
**Wigner-breaking $\mathcal{O}(\delta)$:** $\delta = \frac{1/a_1 - 1/a_0}{1/a_1 + 1/a_0}$
**Wigner-breaking all orders:**

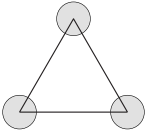

| | Unitary | Wigner | $\mathcal{O}(\delta)$ | $\delta$ all orders |
|---|---|---|---|---|
| LO EFT($\not\pi$) | 1.10 | 1.22 | 1.08/1.19 | 1.14/1.26 |
| $\mathcal{O}(r)$ | 1.42 | 1.66 | 1.58/1.70 | 1.59/1.72 |
| Experiment | | | | 1.5978(40)/1.775(5) |

Table: $^3$H/$^3$He charge radius in unitary and Wigner-limit (Vanasse and Phillips (2016)) arXiv:1607.08585

In Wigner-limit it can be shown both analytically and numerically

$$\mu_{(^3\mathrm{H})} = \mu_p = 2.79\frac{e}{2M_N} \quad , \quad \mu_{(^3\mathrm{He})} = \mu_n = -1.91\frac{e}{2M_N}$$

# Consequences of Wigner-symmetry and Unitarity

**Wigner-limit:** $a_0 = a_1$ and $r_0 = r_1$
**Unitary limit:** $a_0 = a_1 = \infty$
**Wigner-breaking $\mathcal{O}(\delta)$:** $\delta = \frac{1/a_1 - 1/a_0}{1/a_1 + 1/a_0}$
**Wigner-breaking all orders:**

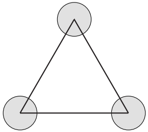

| | Unitary | Wigner | $\mathcal{O}(\delta)$ | $\delta$ all orders |
|---|---|---|---|---|
| LO EFT($\not\pi$) | 1.10 | 1.22 | 1.08/1.19 | 1.14/1.26 |
| $\mathcal{O}(r)$ | 1.42 | 1.66 | 1.58/1.70 | 1.59/1.72 |
| Experiment | | | | 1.5978(40)/1.775(5) |

Table: $^3$H/$^3$He charge radius in unitary and Wigner-limit (Vanasse and Phillips (2016)) arXiv:1607.08585

In Wigner-limit it can be shown both analytically and numerically

$$\mu_{(^3\mathrm{H})} = \mu_p = 2.79\frac{e}{2M_N} \quad , \quad \mu_{(^3\mathrm{He})} = \mu_n = -1.91\frac{e}{2M_N}$$

# Consequences of Wigner-symmetry and Unitarity

**Wigner-limit:** $a_0 = a_1$ and $r_0 = r_1$
**Unitary limit:** $a_0 = a_1 = \infty$
**Wigner-breaking $\mathcal{O}(\delta)$:** $\delta = \frac{1/a_1 - 1/a_0}{1/a_1 + 1/a_0}$
**Wigner-breaking all orders:**

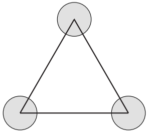

| | Unitary | Wigner | $\mathcal{O}(\delta)$ | $\delta$ all orders |
|---|---|---|---|---|
| LO EFT($\not\pi$) | 1.10 | 1.22 | 1.08/1.19 | 1.14/1.26 |
| $\mathcal{O}(r)$ | 1.42 | 1.66 | 1.58/1.70 | 1.59/1.72 |
| Experiment | | | | 1.5978(40)/1.775(5) |

Table: $^3$H/$^3$He charge radius in unitary and Wigner-limit (Vanasse and Phillips (2016)) arXiv:1607.08585

In Wigner-limit it can be shown both analytically and numerically

$$\mu_{(^3\mathrm{H})} = \mu_p = 2.79\frac{e}{2M_N} \quad , \quad \mu_{(^3\mathrm{He})} = \mu_n = -1.91\frac{e}{2M_N}$$

# Halo-nuclei, something different?

# Halo-Nuclei

- For halo-nuclei $R_{halo} > R_{core}$, can expand in powers of $R_{core}/R_{halo}$.

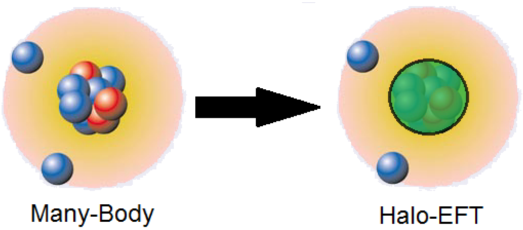


- If a probe has De Broglie wavelength $\lambda$, and $\lambda > R_{core}$ the structure of the core cannot be resolved and it can be treated as a fundamental degree of freedom.
- Breakdown scales of halo-EFT set by $E_{\star}$ (first excited state energy of core), $B_{c-n}$ (one neutron separation energy of core), and $m_{\pi}$

# Halo-Nuclei

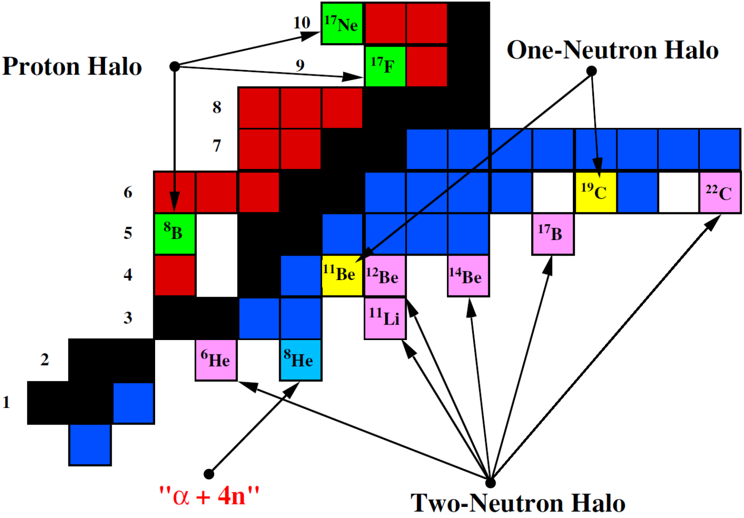


http://www.nupecc.org/report97/report97.pdf

# Halo Trimer Vertex Function

- LO halo-nuclei vertex function given by (Hagen, Hammer, and Platter (2013))

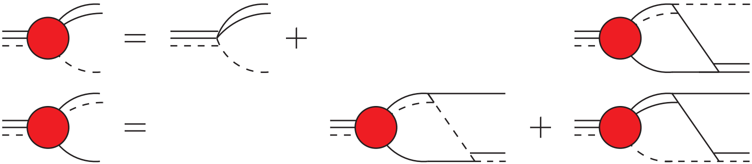

- S-wave interactions in both two and three-body sector
- Nearly identical to pionless EFT
- Differences from pionless EFT: core is spin-0, three-body force chosen differently, and parameters will have different values

# Inputs for Halo Nuclei

- LO interactions are non-perturbative and reproduce neutron-neutron scattering length $a_{nn}$ and neutron-core scattering length $a_{cn}$.
- NLO interactions are perurbative corrections from the neutron-neutron effective range $\rho_{nn}$ and neutron-core effective range $\rho_{cn}$.
- LO and NLO three-body force both fit to two-neutron halo nucleus binding energy.

# Unitary Limit as Benchmark

Calculation of LO halo-nuclei charge radius nearly identical to triton charge radius calculation. In Unitary limit and equal mass limit it is found

| Authors | $mE_{3B}\left\langle r_c^2\right\rangle$ |
|---|---|
| Vanasse | .224 |
| Hagen et al. | .265 |

Using analytical techniques in (Braaten and Hammer (2006)) it can be shown that $mE_{3B}\left\langle r_c^2\right\rangle = (1+s_0^2)/9 \approx .224$ in the unitary and equal mass limit. Changing a single factor in the code of Hagen et al. they would also obtain .224.

# Halo charge-radii

(Vanasse (2016)) arXiv:1609.08552

| Nucleus | $\langle r_C^2 \rangle_0$ fm$^2$ | $\langle r_C^2 \rangle_{0+1}$ fm$^2$ | $\langle r_C^2 \rangle$-Exp. fm$^2$ |
|---|---|---|---|
| $^{11}$Li | 0.744(275) | 0.774(106) | 1.171(120) [6]<br>1.104(85) [5]<br>0.82(11) [1, 2] |
| $^{14}$Be | 0.126(98) | 0.134(81) | — |
| $^{22}$C | $0.520^{+\infty}_{-0.274}$ | $0.530^{+\infty}_{-0.283}$ | — |

Table: LO and NLO halo-EFT predicitions for charge radii of two-neutron halo nuclei. Included are existing experimental results. The NLO results use the naturalness estimate $\rho_{cn} \sim 1/m_\pi \sim 1.4$ fm for the NLO prediction, where $\rho_{cn}$ is the effective range for $cn$ scattering.

# Halo matter-radii

(Vanasse (2016)) arXiv:1609.08552

| Nucleus | $\langle r_M^2 \rangle_0$ fm$^2$ | $\langle r_M^2 \rangle_{0+1}$ fm$^2$ | $\langle r_M^2 \rangle$-Exp. fm$^2$ |
|---|---|---|---|
| $^{11}$Li | $5.76 \pm 2.13$ | $6.05 \pm 0.83$ | $5.34 \pm 0.15$ [4] |
| $^{14}$Be | $1.23 \pm 0.96$ | $1.34 \pm 0.81$ | $4.24 \pm 2.42$ [4]<br>$2.90 \pm 2.25$ [4] |
| $^{22}$C | $9.00^{+\infty}_{-5.01}$ | $9.22^{+\infty}_{-5.16}$ | $21.1 \pm 9.7$ [3, 7]<br>$3.77 \pm 0.61$ [3, 8] |

Table: LO and NLO halo-EFT predicitions for mater radii of two-neutron halo nuclei. Included are existing experimental results. The NLO results use the naturalness estimate $\rho_{cn} \sim 1/m_\pi \sim 1.4$ fm for the NLO prediction, where $\rho_{cn}$ is the effective range for $cn$ scattering.

# nd Scattering Results

(Margaryan,Springer, and Vanasse (2015)) arXiv:1510.07598

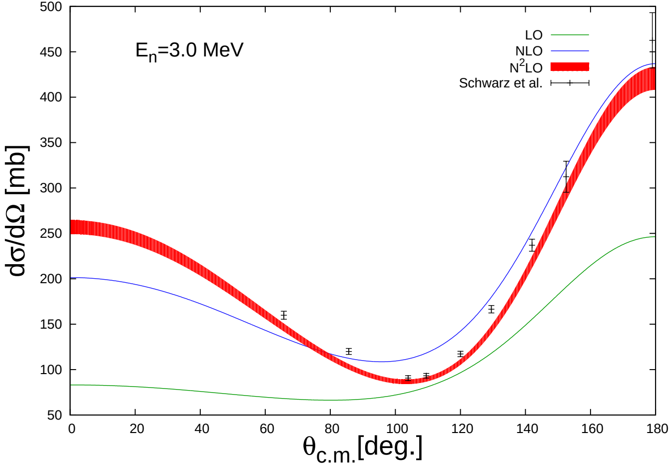

# Nd polarization Observables

$$A_y = \frac{\frac{d\sigma}{d\Omega\uparrow}^{(\mathrm{N^3LO})} - \frac{d\sigma}{d\Omega\downarrow}^{(\mathrm{N^3LO})}}{2\frac{d\sigma}{d\Omega}^{(\mathrm{NNLO})}}$$

- At $\mathrm{N^3LO}$ new three-body force occurs that cancels in numerator of $A_y$.
- Position of maximum of $A_y$ is determined by minimum of scattering cross section which is only reproduced well at NNLO.
- $A_y$ is dominated by ${}^3P_J$ two-body interactions, while two-body $SD$-mixing contribution is negligible.
- Two-body $P$-wave interaction LECs fit to phase shifts via

$$T^{{}^3P_J}(p) = \frac{M_N p}{4\pi}\delta^{{}^3P_J}(p)$$

# nd Polarization Observables

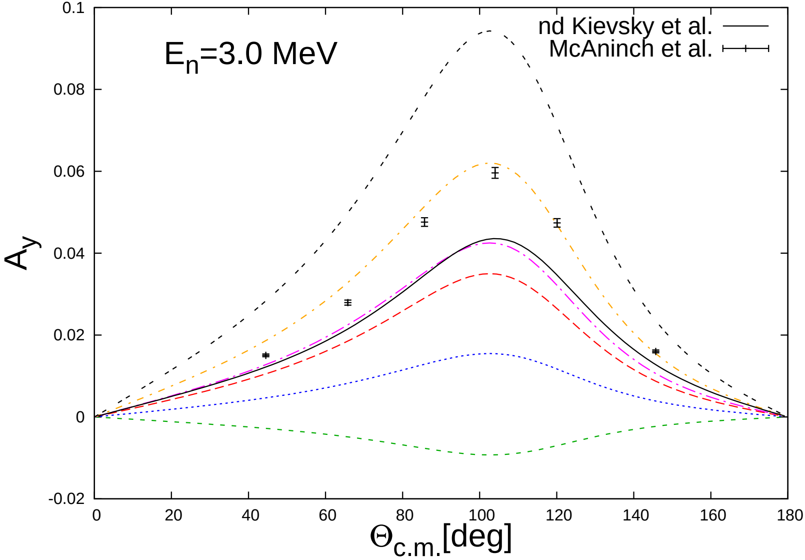

# Conclusions and Future directions

- Charge radii of $^3$H and $^3$He reproduced well at NNLO in EFT($\not\pi$).
- Magnetic moments reproduced within errors at LO in EFT($\not\pi$).
- Wigner-symmetry gives good expansion for charge radii and is interesting limit for magnetic moments of $^3$H and $^3$He.
- Reproduce analytical results in unitary and equal mass limit for charge radii of halo nuclei. Should be used as benchmark for all such calculations.
- Further theoretical and experimental work is necessary in halo-nuclei to measure charge-radii and reduce error in other measurements. Determine value for $\rho_{cn}$.
- Add resonant two-body $P$-wave interactions to investigate $^6$He and $^{17}$B two-neutron halo-nuclei

[1] H. Esbensen, K. Hagino, P. Mueller, and H. Sagawa.
Charge radius and dipole response of Li-11.
*Phys. Rev.*, C76:024302, 2007.

[2] T. Nakamura et al.
Observation of Strong Low-Lying E-1 Strength in the Two-Neutron Halo Nucleus Li-11.
*Phys. Rev. Lett.*, 96:252502, 2006.

[3] A. Ozawa et al.
Measurements of interaction cross sections for light neutron-rich nuclei at relativistic energies and determination of effective matter radii.
*Nucl. Phys.*, A691:599–617, 2001.

[4] A. Ozawa, T. Suzuki, and I. Tanihata.
Nuclear size and related topics.
*Nucl. Phys.*, A693:32–62, 2001.

[5] M. Puchalski, A. M. Moro, and K. Pachucki.
Isotope Shift of the S-31/22- S-21/22 Transition in Lithium and the Nuclear Polarizability.
*Phys. Rev. Lett.*, 97:133001, 2006.

[6] R. Sanchez et al.
Nuclear Charge Radii of Li-9, Li-11: The Influence of Halo Neutrons.
*Phys. Rev. Lett.*, 96:033002, 2006.

[7] K. Tanaka et al.
Observation of a Large Reaction Cross Section in the Drip-Line Nucleus C-22.
*Phys. Rev. Lett.*, 104:062701, 2010.

[8] Y. Togano, T. Nakamura, Y. Kondo, J. Tostevin, A. Saito, J. Gibelin, N. Orr, N. Achouri, T. Aumann, H. Baba, F. Delaunay, P. Doornenbal, N. Fukuda, J. Hwang, N. Inabe, T. Isobe, D. Kameda, D. Kanno, S. Kim, N. Kobayashi, T. Kobayashi, T. Kubo, S. Leblond, J. Lee, F. Marqus, R. Minakata, T. Motobayashi, D. Murai, T. Murakami, K. Muto, T. Nakashima, N. Nakatsuka, A. Navin, S. Nishi, S. Ogoshi, H. Otsu, H. Sato, Y. Satou, Y. Shimizu, H. Suzuki, K. Takahashi, H. Takeda, S. Takeuchi, R. Tanaka, A. Tuff, M. Vandebrouck, and K. Yoneda.
Interaction cross section study of the two-neutron halo nucleus 22c.
*Physics Letters B*, pages –, 2016.

# nd Polarization Observables

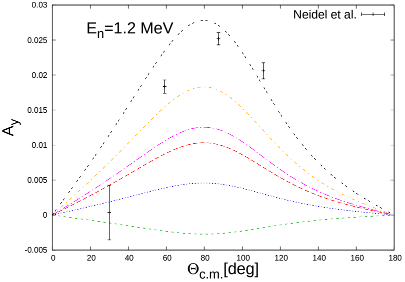


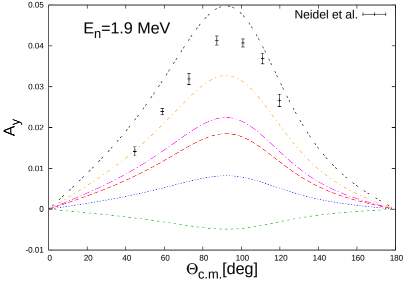


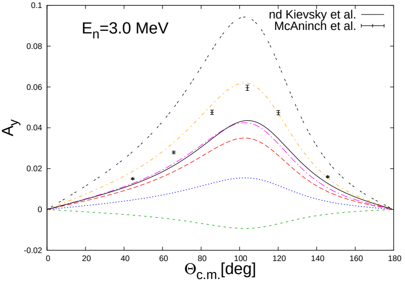

# nd Polarization Observables

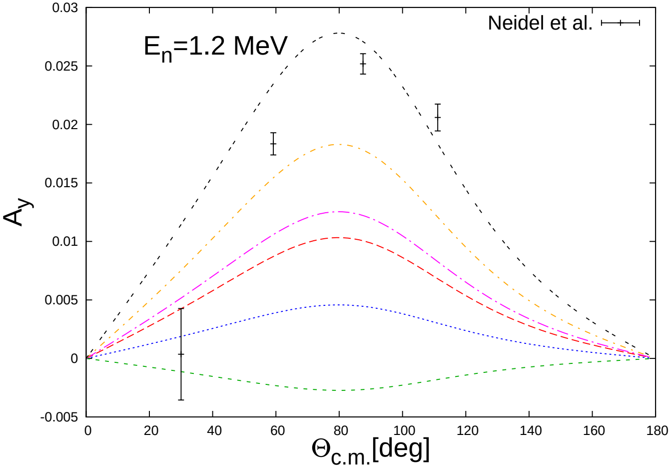

# nd Polarization Observables

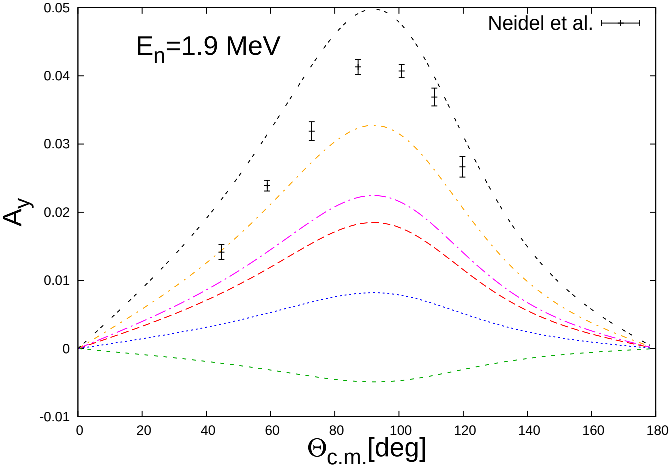

# "nd" Polarization Observables